


Synoptic environments and characteristics of cold air outbreaks in the Irminger Sea

Journal Article**Author(s):**

Papritz, Lukas 

Publication date:

2017-08

Permanent link:

<https://doi.org/10.3929/ethz-b-000379989>

Rights / license:

In Copyright - Non-Commercial Use Permitted

Originally published in:

International Journal of Climatology 37(51), <https://doi.org/10.1002/joc.4991>

Synoptic environments and characteristics of cold air outbreaks in the Irminger Sea

Lukas Papritz^{1*}

¹*Geophysical Institute, University of Bergen and Bjerknes Centre for Climate Research, Bergen, Norway*

**Corresponding author address:*

Lukas Papritz, Geophysical Institute, University of Bergen and Bjerknes Centre for Climate Research, Allegaten 70, Postboks 7803, 5020 Bergen, Norway

E-Mail: lukas.papritz@uib.no

ABSTRACT

Cold air outbreaks (CAOs) are the dominant cause of intense wintertime upward heat fluxes in the Irminger Sea. In this study, the climatological pathways of Irminger Sea CAO airmasses and the evolution of airmass properties, as well as the large-scale synoptic environments leading to CAO formation are examined for winter. To that end, a comprehensive, multi-decadal climatology of Irminger Sea CAO airmasses using kinematic trajectories is presented, complemented by a composite analysis of the large-scale synoptic environment for intense CAO events.

The following three synoptic environments conducive for CAO formation are identified: (i) The westerly environment is characterised by an upper-level trough crossing Greenland and inducing strong westerly winds at crest level, accompanied by either cyclogenesis or the intensification of an existing cyclone in the lee of Greenland. The associated CAO airmasses originate in the Canadian Arctic, overflow southern Greenland, and descend into the Irminger Sea with an according imprint in their thermodynamic evolution. (ii) In the easterly cyclonic environment, one or multiple cyclones in the Nordic Seas induce northerly winds along Greenland's eastern coast that transport Arctic airmasses from Fram Strait to Denmark Strait. (iii) The easterly anti-cyclonic environment, finally, is dominated by an anti-cyclone over Greenland with similar airmass origins and pathways as in the easterly cyclonic environment. The two easterly environments represent the limiting cases of an intermediate spectrum, whereas in contrast the westerly environment is clearly distinct. Katabatic drainage from northern Greenland contributes to the CAO airmasses in both easterly environments, whereas in

25 the easterly cyclonic environment also marine airmasses from the Nordic Seas are
26 involved. An important conclusion of this study is that the amount of heat ex-
27 tracted from the ocean by a CAO airmass depends critically on its pathway, and
28 thus on the synoptic environment.

1 Introduction

The Irminger Sea encompasses the waters that extend from Cape Farewell – the southernmost tip of Greenland – to Iceland (see Fig. 1 for location names). During winter it is a region of highly variable, in many aspects extreme, climatic conditions: It comprises the stormiest portions of the world’s oceans with globally the highest frequency of near-surface wind speeds in excess of 20 m s^{-1} (Sampe and Xie, 2007). In addition to that, it is a breeding ground for extratropical cyclones, many of them propagating north-eastwards into the Nordic and Barents seas – a peculiarity reflected in a high rate of lee cyclogenesis (Wernli and Schwierz, 2006; Dacre and Gray, 2009). Furthermore, recent evidence has revived the long existent notion that heat losses to the atmosphere in the Irminger Sea contribute to the formation of North Atlantic Deep Water (Nansen, 1912; Pickart et al., 2003a,b; Våge et al., 2009b, 2011), which constitutes the deep limb of the Atlantic meridional overturning circulation. The exchanges of heat across the atmosphere – ocean interface in the Irminger Sea, therefore, have climatic influences far beyond the region itself (cf. Buckley and Marshall, 2016). As a consequence, a detailed understanding of the processes shaping air-sea heat fluxes is highly relevant for understanding the complex climate of the North Atlantic as a whole.

In this study, I focus on a particular type of wintertime weather event that plays a key role in controlling air-sea heat exchanges: marine cold air outbreaks (CAOs). In fact, CAOs account for more than 80 % of the wintertime oceanic heat loss over most parts of the Irminger Sea (Papritz and Spengler, 2016). Previously, Irminger Sea CAOs have been investigated in the context of climatological studies addressing CAOs over the entire north-east Atlantic (Kolstad et al., 2009;

53 Papritz and Spengler, 2016); still fundamental questions regarding the synoptic
54 conditions leading to their formation, as well as their characteristics remain, as I
55 aim to outline in the following.

56 Based on a composite analysis, Kolstad et al. (2009) found that Irminger Sea
57 CAOs typically occur in the presence of a deep Icelandic Low with its center
58 over the Irminger Sea, and an upper-level trough slightly displaced to the west.
59 This configuration of the large-scale flow leads to the transport of cold airmasses
60 from the Canadian Arctic into the Labrador Sea basin. Consequently, CAOs in
61 the Irminger Sea are often concomitant with CAOs in the Labrador Sea (Kolstad
62 et al., 2009). The configuration of the flow suggests further that Irminger Sea CAO
63 airmasses originate from the Labrador Sea sector. Kolstad et al. (2009) also noted
64 a particular case (their case 8), however, where northerly winds over Denmark
65 Strait brought cold airmasses into the Irminger Sea region.

66 Indeed, calculations of kinematic trajectories revealed that climatologically
67 two pathways of airmasses leading to CAO formation in the Irminger Sea exist,
68 a *western* and an *eastern* pathway (Papritz and Spengler, 2016). Accordingly,
69 in this study I will refer to CAOs formed by airmasses following the western
70 or eastern pathways as westerly or easterly CAOs, respectively. The airmasses of
71 westerly CAOs originate over the Canadian Arctic and the Labrador Sea, overflow
72 the plateau of southern Greenland, and descend as downslope flows. In contrast,
73 most of the airmasses of easterly CAOs have their origin in the Arctic basin fol-
74 lowing Greenland's eastern coast from Fram Strait southward with contributions
75 of katabatic drainage from Greenland's plateau, as well as from the Nordic Seas.
76 The existence of these two pathways indicates that a richer spectrum of synoptic
77 conditions can induce CAOs in the Irminger Sea than the composite analysis by

78 Kolstad et al. (2009) suggests. Hence, it is one of my main goals to elucidate the
79 large-scale environments leading to CAO formation in the Irminger Sea.

80 The large-scale flow over and east of Greenland is dominated by Greenland
81 blocking (e.g., Hanna et al., 2016), which is characterized by a quasistationary
82 anticyclone over Greenland, the north-eastern branch of the North Atlantic storm
83 track, and cyclogenesis in the lee of Greenland (Dacre and Gray, 2009). The anti-
84 cyclonic flow associated with Greenland blocking provides steady northerly winds
85 along Greenland's eastern coast, favorable for the long-range transport of Arctic
86 airmasses contributing to easterly CAOs. However, a sequence of consecutive
87 cyclones might also provide such transport, e.g., when one storm that propagated
88 into the Nordic Seas is followed by another storm in the Irminger Sea. Thus, the
89 relative importance of Greenland anti-cyclones and cyclones in the Nordic Seas
90 for the formation of easterly CAOs remains an open question.

91 At sub-synoptic scale, the intense interaction of the large-scale flow with
92 Greenland's steep coastal orography and the 3000 m high ice sheet leads to a
93 variety of high wind speed phenomena. Among them are barrier winds asso-
94 ciated with promontories along Greenland's coast in the northern portions of
95 the Irminger Sea and Denmark Strait (e.g., Petersen et al., 2009; Harden et al.,
96 2011; Harden and Renfrew, 2012), as well as westerly tip jets south-east of Cape
97 Farewell (Doyle and Shapiro, 1999; Moore and Renfrew, 2005; Moore et al., 2008;
98 Våge et al., 2009a). Furthermore, katabatically enforced downslope winds bring
99 cold airmasses from the ice sheet down into the Irminger Sea, for example, in
100 the Ammassalik valley (Heinemann and Klein, 2002; Oltmanns et al., 2014). The
101 ocean can lose tremendous amounts of heat during such high wind speed events.
102 For example, Oltmanns et al. (2014) estimated that up to 20 % of the winter-

103 time heat loss in the Irminger Sea occurs in association with intermittent downs-
104 lope wind storms. Furthermore, Harden et al. (2011) found surface turbulent heat
105 fluxes to exceed 400 W m^{-2} during certain events of barrier winds. They pointed
106 out that the magnitude of air-sea heat fluxes during barrier wind events is con-
107 trolled by the air-sea temperature difference, with high heat fluxes only when the
108 air is significantly colder than the ocean, that is in the presence of an intense CAO.

109 Following the approach by Papritz and Spengler (2016), I make use of kine-
110 matic trajectories that sample wintertime CAO airmasses in the Irminger Sea to

- 111 1. characterise the synoptic environments in which westerly and easterly CAOs
112 form;
- 113 2. analyse the Lagrangian evolution of characteristic properties of these air-
114 masses; and
- 115 3. quantify the amount of heat extracted from the ocean.

116 The article is structured as follows: In section 2 I outline the method to obtain
117 the trajectory data set, followed in section 3 by three case studies of CAOs in
118 the Irminger Sea, two of which are of the easterly and one of the westerly CAO
119 type. These case studies are followed in section 4 by a climatological account
120 of the characteristics of Irminger Sea CAO airmasses, an analysis of the synoptic
121 environments in which they form, and a quantification of the sensible and latent
122 heat extracted from the ocean by the CAO airmasses. I conclude with a synthesis
123 of the results in section 5.

124 **2 Methodology**

125 **2.1 Reanalysis and cyclone data sets**

126 The analyses presented in this study are based on the Interim reanalysis (ERA-
127 Interim) from the European Centre for Medium-Range Weather Forecasts (ECMWF;
128 Dee et al., 2011) for extended winters (November – April) in the period 1979 to
129 2014. The data is available at 6-hourly temporal resolution and on 60 vertical lev-
130 els. In the horizontal it is interpolated from the original T255 spectral resolution
131 to a $1^\circ \times 1^\circ$ longitude–latitude grid. Surface turbulent heat fluxes are obtained
132 from model forecast steps 9 to 21 and averaged over 6-hourly windows centred on
133 synoptic times.

134 In order to quantify how often cyclones are involved in CAO formation, I make
135 use of the sea level pressure based cyclone identification method by Wernli and
136 Schwerz (2006). This method yields for each time step a binary field indicating at
137 each grid point whether it is affected by the presence of a cyclone or not. Thereby,
138 the area affected by a cyclone is determined by the outermost closed contour of
139 sea level pressure surrounding one or several pressure minima but no maxima.
140 Furthermore, the maximum contour length is limited to 7'500 km. Averaging of
141 the binary cyclone fields over a specific set of time steps yields the respective
142 frequency of cyclones. In addition, cyclone centers, each defined as the deepest
143 minimum within a sea level pressure contour, are tracked using an updated version
144 of the tracking algorithm by Wernli and Schwerz (2006). I use these cyclone
145 tracks to identify cyclogenesis events in the Irminger Sea.

146 2.2 Compilation of CAO trajectory data set

147 Kinematic trajectories are calculated with the aid of the LAGRangian ANalysis
148 TOol (LAGRANTO; Sprenger and Wernli, 2015), which uses the three dimen-
149 sional winds from ERA-Interim as input. The starting region of the trajectories
150 encompasses the waters in the lee of Greenland that extend from Cape Farewell to
151 Denmark Strait and Iceland (cf. Fig. 1). Trajectory starting positions are defined
152 on a regular grid with $80\text{ km} \times 80\text{ km}$ horizontal grid spacing on 21 equidistant
153 vertical levels ranging from 1000 hPa to 500 hPa. Accordingly, each trajectory
154 represents a mass of $\sim 1.6 \cdot 10^{12}\text{ kg}$.

155 The compilation of the trajectory data set is undertaken in three main steps:

- 156 1. Initial grid points are defined to comprise all points of the starting grid that
157 lie within the starting area and satisfy $\theta_{\text{SKT}} - \theta > 4\text{ K}$, where θ and θ_{SKT}
158 denote potential temperature and potential skin temperature, respectively.
159 The initial grid points are further required to be neither covered by land nor
160 sea ice, i.e., fractional land and sea ice cover must be below 50 %.
- 161 2. Trajectories are calculated from the initial grid points backward in time for
162 a duration of 6 h. If at the previous synoptic time the trajectory is not con-
163 sidered a CAO, i.e., $\theta_{\text{SKT}} - \theta \leq 0\text{ K}$ at $t = -6\text{ h}$, the trajectory is retained,
164 otherwise it is discarded. By virtue of this criterion a double sampling of
165 the same CAO airmass by more than one trajectory is avoided.
- 166 3. The retained trajectories are extended forward and backward in time to span
167 the time interval $-192\text{ h} \leq t \leq 144\text{ h}$, such as to encompass the pre-
168 conditioning of the CAO airmass, as well as the entire lifetime of the CAO.

169 In addition, wind speed, temperature, and surface turbulent heat fluxes are
170 traced along trajectories by interpolating these fields to the respective tra-
171 jectory positions.

172 In this study, I only consider trajectories with $\theta_{\text{SKT}} - \theta > 4 \text{ K}$ at $t = 0 \text{ h}$. Hence, I
173 exclude weak CAO airmasses, which are frequent but have a limited impact on air-
174 sea heat exchanges (Papritz et al., 2015; Papritz and Spengler, 2016). A sensitivity
175 analysis revealed that the results presented in this study are rather insensitive to
176 the precise choice of the threshold (not shown). Furthermore, only airmasses
177 associated with the formation of a CAO in the Irminger Sea are included in the
178 analysis, whereas CAO airmasses satisfying $\theta_{\text{SKT}} - \theta > 4 \text{ K}$ elsewhere but being
179 advected into the Irminger Sea are not considered.

180 Finally, I introduce three notions that will facilitate the subsequent discussion
181 of the results. The time of CAO formation, i.e., $t = 0 \text{ h}$., is referred to as the
182 *basetime*, and the *rate of CAO formation* is defined as the number of trajectories
183 newly satisfying $\theta_{\text{SKT}} - \theta > 4 \text{ K}$ per 6 hours. Furthermore, the continuous time
184 period beginning at $t = 0 \text{ h}$ and for which $\theta_{\text{SKT}} - \theta > 0 \text{ K}$ is denoted by the *CAO*
185 *phase* of a trajectory.

186 **3 Case studies**

187 Here, I will illustrate typical pathways of CAO airmasses and corresponding syn-
188 optic situations. To that end, I consider three case studies, a westerly CAO (case
189 A) and two easterly CAOs with differing synoptic situations (cases B and C). I
190 focus on the peak of the events, i.e., the time step when the rate of CAO formation
191 is maximum. For the sake of clarity, I only display trajectories whose basetime

192 corresponds to the time of the peak of the event.

193 **3.1 Case A: 16 February 2005**

194 In case A the upper-level flow is dominated by the passage of an upper-level
195 trough over southern Greenland, which induces lee cyclogenesis (Fig. 2a). Fur-
196 thermore, an anti-cyclone is located west of the British Isles. Two days before
197 CAO formation, most of the air parcels are located south-west of Baffin Island,
198 which are then advected into the Labrador Sea below the upper-level trough. As
199 the trough crosses Greenland, they ascend on its rearward flank over southern
200 Greenland, and subsequently descend along the steep coastline into the Irminger
201 Sea. As the air parcels flow over southern Greenland, their trajectory shows typ-
202 ical features of rotational flows past large mountains (cf. Petersen et al., 2003),
203 namely deceleration and poleward deflection on the upstream side, decreasing
204 vorticity during ascent with anti-cyclonic curvature on the mountain crest, and
205 increasing vorticity as they descend.

206 After CAO formation, the strong pressure gradient over the Irminger and Nor-
207 wegian seas, established by the anti-cyclone over the British Isles and the lee-
208 cyclone, causes a rapid advection of the air parcels towards the coast of middle and
209 northern Norway, whereby the air-parcel trajectories remain coherent (Fig. 2b).
210 As a consequence of the north-eastward translation of the lee cyclone towards
211 Svalbard, a substantial fraction of the air parcels is caught by the cyclonic flow
212 and advected into the interior Arctic and the Barents Sea.

213 **3.2 Case B: 9 December 1981**

214 In case B an intense and persistent anti-cyclone centered over Greenland leads to
215 a coherent, deep transport of cold airmasses from Fram Strait along Greenland's
216 east coast into the Irminger Sea (Fig. 2c). The trajectories show that the drainage
217 of radiatively cooled airmasses from northern Greenland enhances this cold air
218 flow. A number of air parcels overflow Iceland prior to CAO formation. Accord-
219 ingly, CAO formation takes place over Denmark Strait and off the south-western
220 coast of Iceland.

221 A peculiarity of the flow configuration is a saddle point in sea level pressure
222 located over the central North Atlantic, which occurs because the anti-cyclone
223 over Greenland is flanked by cyclonic circulations; specifically at peak time a
224 cyclonic disturbance is located close to Newfoundland and a broad trough is found
225 over Scandinavia (Fig. 2c). Consequently, a bifurcation occurs and the air parcels
226 are diverted in opposite directions after CAO formation (Fig. 2d). A bundle of
227 trajectories reaches Canada north of Newfoundland, whereas another bundle is
228 directed towards the British Isles.

229 **3.3 Case C: 29 December 2012**

230 In contrast to case B, the anti-cyclone over Greenland is much less pronounced in
231 case C. Instead, the dominating large-scale features are upper-level wave breaking
232 over the eastern North Atlantic and an associated deep cyclone with its center lo-
233 cated south-east of Iceland (Fig. 2e). The cyclonic circulation gives rise to strong
234 north-easterlies over Denmark Strait, conducive for barrier winds (Harden et al.,
235 2011), whereas further north along Greenland's coast, northerlies are restricted

236 to the coastal areas. The spatial distribution of CAO air parcels prior to CAO
 237 formation shows large scatter and the trajectories are less coherent than in case
 238 B. Three main bundles of air parcels are discernible: first, the main bundle of
 239 air parcels originates in the Arctic and over northern Greenland, with trajectories
 240 akin to those of case B, but restricted to the vicinity of coastal Greenland; second,
 241 cold drainage flows from south-eastern Greenland descend into the Irminger Sea
 242 near Denmark Strait; and third, a bundle of marine air parcels is advected into
 243 the Irminger Sea by the cyclonic circulation over the Nordic Seas. After CAO
 244 formation, the air parcels contribute to the cold sector of the cyclone and they are
 245 advected towards Scotland and southern Norway (Fig. 2f). Furthermore, a number
 246 of air parcels also recirculate into the Nordic Seas.

247 **4 Climatological perspective on Irminger Sea CAOs**

248 The three cases of Irminger Sea CAOs presented in the previous section are archety-
 249 pal, as I aim to corroborate in the following from a climatological perspective. I
 250 do this by examining the climatological pathways and Lagrangian characteristics
 251 of Irminger Sea CAO airmasses and by investigating the composite large-scale
 252 environments in which these CAOs form.

253 **4.1 Westerly and easterly CAO trajectories**

254 I stratify CAO trajectories into westerly and easterly ones according to longitude
 255 two days prior to CAO formation, i.e., at $t = -48$ h. If at this time a specific
 256 trajectory is located to the west (east) of Cape Farewell, 43° W, it is considered
 257 a westerly (easterly) trajectory. This criterion provides a clear-cut separation of

trajectories following the westerly and easterly pathways, respectively, as is confirmed by maps of the climatological mean horizontal mass fluxes (Figs. 3a, b). Note that the horizontal mass flux associated with a single trajectory is given by $M \cdot \mathbf{u}$, where $M \approx 1.6 \cdot 10^{12}$ kg denotes its mass and \mathbf{u} its horizontal wind vector. By virtue of the hydrostatic relation, the horizontal mass fluxes can be expressed in units of hPa m s^{-1} .

Westerly CAO airmasses have their origin over Labrador and Baffin Island, subsequently move into the Labrador Sea and then overflow southern Greenland with CAO formation along Greenland's south-eastern coast (Fig. 3a). Undulations of mass flux vectors over and around Greenland hint at similar air parcel trajectories in the climatology as in case A, reflecting changes of relative vorticity associated with the overflow of Greenland. On the downslope side of Greenland, the mass fluxes are most intense in the Ammassalik area and over the southernmost tip of Greenland.

Easterly CAO airmasses originate largely in the interior Arctic but are enhanced by cold drainage flows from northeastern Greenland, as well as by cold airmasses from the Barents Sea (Fig. 3a). Airmasses originating over the Nordic Seas, as in case C, however, are rather atypical. In contrast to westerly CAOs, the formation of easterly CAOs occurs in the northern parts of the Irminger Sea, namely over Denmark Strait – as off-ice flow – as well as off the coast of southwestern Iceland (Fig. 3b).

After CAO formation, westerly CAO airmasses are advected eastwards towards the British Isles, Norway, as well as the Barents Sea (Fig. 3c). For easterly CAOs, however, the climatology shows a splitting of CAO airmass fluxes, towards the British Isles and the southern Labrador Sea, but with the more intense

283 fluxes directed towards the east (Fig. 3d). Furthermore, easterly CAO airmasses
284 are transported less far to the north than westerly airmasses.

285 **4.2 Characteristics of CAO airmasses**

286 Figure 4a shows the pressure distribution of westerly and easterly CAO trajec-
287 ries. About 50 % of the westerly CAO trajectories do not show substantial as-
288 cent before descending into the Irminger Sea. These non-ascending trajectories
289 originate in the free troposphere above the inversion layer of a CAO airmass in
290 the Labrador Sea. Interestingly, also about 25 % of the easterly CAO trajec-
291 ries descend by more than 200 hPa with no previous ascent before. They largely
292 represent radiatively cooled airmasses originating from the plateau of northern
293 Greenland.

294 High wind speeds strongly enhance surface fluxes of sensible and latent heat.
295 Given the prevalence of high wind speed events in the Irminger Sea, it is, there-
296 fore, interesting to look at the distribution of wind speeds, as evident from the
297 kinetic energy distribution, among westerly and easterly CAO trajectories. West-
298 erly CAO trajectories are accelerated while they descend into the Irminger Sea
299 (Fig. 4b). Doyle and Shapiro (1999) suggested that this acceleration is owed to
300 Bernoulli conservation. However, it is conceivable that, for example, the down-
301 ward mixing of momentum contributes too. The maximum 90th-percentile spe-
302 cific kinetic energy amounts to about $330 \text{ m}^2 \text{ s}^{-2}$, corresponding to $\approx 26 \text{ m s}^{-1}$ – a
303 typical value for westerly tip jets (Våge et al., 2009a). High wind speeds among
304 easterly CAO trajectories, in contrast, are the result of barrier flow (cf. Harden
305 et al., 2011). The highest median and 75th-percentile specific kinetic energy

among easterly CAO trajectories remain below those of westerly CAOs, whereas the 90th-percentile is almost of the same magnitude as for westerly CAOs. It is noteworthy that in both categories the highest specific kinetic energy is observed at the time of or immediately after CAO formation, indicating that high wind speeds enhance air-sea heat exchanges in these CAO airmasses.

The contributions of diabatic heating and cooling, and adiabatic temperature changes associated with vertical motion to the thermodynamic evolution of CAO airmasses can be investigated via a potential temperature – temperature ($\theta - T$) diagram (Fig. 5). To facilitate the comparison of temperatures and relative temperature changes for different CAO airmasses, I display the diagrams both in terms of absolute (Fig. 5a) and relative values (Fig. 5b). In addition, I divide westerly CAO trajectories into subsets of ascending and non-ascending trajectories owing to their spread in the vertical before crossing Greenland. Trajectories with a pressure at $t = -48$ h above and below the median among all westerly CAO trajectories are considered as ascending and non-ascending, respectively.

Ascending westerly CAO trajectories are cooled diabatically until about 36 h before CAO formation. Subsequently, the trajectories are exposed to open ocean in the Labrador Sea. Thereby, the positive air-sea potential temperature difference results in diabatic warming due to intense surface sensible heat fluxes, and, provided sufficient uptake of moisture, the release of latent heat as the trajectories ascend over Greenland. The increase of temperature associated with diabatic warming, however, is overcompensated by adiabatic cooling due to ascent. Non-ascending trajectories, in contrast, are initially potentially warmer and undergo substantial diabatic cooling until they begin to descend about 12 h prior to CAO formation. As the trajectories are located in the free troposphere, both radiation

331 and evaporation at the top of a cloud layer are processes that can account for the
332 diabatic cooling. Temperature increases by about 18 K in the median as the tra-
333 jectories descend in the lee of Greenland.

334 Initially potentially colder than non-ascending westerly CAO trajectories, east-
335 erly CAO trajectories are subject to less diabatic cooling. Nevertheless, they show
336 a temperature increase of about 10 K – a signature of descent during the 48 h
337 prior to CAO formation. This warming is due to airmasses drained from north-
338 ern Greenland, which merge with the southbound stream of CAO airmasses along
339 Greenland’s eastern coast. However, diabatic warming also contributes slightly
340 to this temperature increase, indicating that some trajectories are exposed to open
341 ocean in the Greenland and Iceland seas, and hence to surface heat fluxes already
342 before CAO formation in the Irminger Sea.

343 During the CAO phase, which in the median lasts about 30 h for westerly and
344 42 h for easterly CAOs, trajectories warm substantially due to surface sensible heat
345 fluxes and latent heat release. While westerly and easterly CAO trajectories are
346 warmed at similar rates during the first 24 h after CAO formation, easterly CAO
347 trajectories are subject to more diabatic warming over the entire CAO phase than
348 westerly ones. Furthermore, ascending westerly CAO trajectories are heated more
349 than non-ascending ones due to lower potential temperature at $t = 0$ h, and hence
350 stronger surface sensible heat fluxes. As I will discuss later, there are differences
351 in the θ – T curves of easterly CAO trajectories depending on the precise pathways
352 of the airmasses, and therefore the synoptic environment.

353 4.3 Identification of CAO events

354 Figure 6a shows an example timeseries of the rates of CAO formation for extended
355 winter 2009 / 2010. Several periods of continuously enhanced formation rates are
356 evident, each of them showing one or several pronounced peaks indicating CAO
357 events. Specifically, I define CAO events as follows: First, local maxima of the
358 formation rate timeseries exceeding the 95th-percentile in the study period are
359 identified. The 95th-percentile threshold ensures that only particularly intense
360 CAO events are selected. Second, several such maxima occurring within a 2-day
361 window are clustered on the most intense maximum with the weaker ones being
362 removed. The remaining maxima define the CAO events.

363 The number of CAO events in the Irminger Sea increases gradually during
364 the first three winter months (Fig. 6c). It remains high until March and falls off
365 steeply in April. Westerly CAOs are most frequent in February, the coldest month
366 of the year, whereas easterly CAOs are most frequent in January and March with
367 a minimum in February. It is important to note that, owing to the large inter-
368 annual variability, this February minimum is not a statistically robust feature and
369 a corroboration would require longer timeseries. In fact, only 12 out of 35 winters
370 feature a lower number of events in February than in both January and March.

371 On average there are 15.3 so defined CAO events per extended winter, where-
372 off 7.3 are of the westerly and 8 of the easterly type, yielding a total of 254 west-
373 erly and 280 easterly CAO events in the study period. The inter-annual variability
374 is substantial, however, with a minimum of 6 events in winters 1984 / 1985 and
375 2002 / 2003, and a maximum of 27 events in 1982 / 1983 (Fig. 6b). The yearly
376 numbers of westerly and easterly events are only weakly correlated ($r = 0.34$),

377 indicating that the formation of westerly and easterly CAOs is subject to very
378 different large-scale conditions.

379 The North Atlantic Oscillation (NAO), characterized by the pressure differ-
380 ence between Stykkisholmur (Iceland) and Lisbon (Portugal), is the principal
381 mode of large-scale variability over the North Atlantic (e.g., Wanner et al., 2001),
382 potentially with a strong influence on the formation of CAOs in the Irminger Sea.
383 For example, a case study of the negative NAO winter 2010 suggests that the NAO
384 exerts some control on the occurrence of CAOs in the Labrador and Irminger seas
385 via its association with anomalous cyclone frequency near Iceland (Woollings
386 et al., 2016). Using the normalized NAO index by Hurrell (1995), the number
387 of westerly CAO events per extended winter is weakly correlated with the NAO
388 index averaged over the same months ($r = 0.41$). This suggests that the formation
389 of westerly CAOs is more frequent in winters with an enhanced cyclone activity
390 near Iceland and in the Irminger Sea. In contrast, no substantial correlation ex-
391 ists for easterly CAOs ($r = 0.17$), indicating that modes of variability other than
392 the NAO, such as, for example, the Iceland - Lofoten dipole in cyclone activity
393 (Jahnke-Bornemann and Brümmer, 2009) play a more important role for these.
394 These rather modest and low correlations for westerly and easterly CAOs, respec-
395 tively, are in contrast to the comparatively high correlations of a CAO index with
396 the NAO (up to $r = 0.7$ in the western Irminger Sea) as found by Kolstad et al.
397 (2009). However, their analysis indicates somewhat weaker correlations closer to
398 Denmark Strait, the preferred formation region of easterly CAOs. Furthermore,
399 it is likely that weaker CAOs than the events considered here, are less dependent
400 on modes of variability other than the NAO that favor the meridional, long-range
401 transport of very cold Arctic airmasses.

4.4 Synoptic environments

4.4.1 Composites

In order to elucidate the synoptic environments in which westerly and easterly CAOs form, I consider lag composites of 500 hPa geopotential height and sea level pressure for westerly (Figs. 7a - e) and easterly (Figs. 7f - k) CAO events.

One day before the peak of a westerly CAO event, the center of an upper-level trough is located to the west of Greenland (Fig. 7a). As in case A, the upper-level trough subsequently extends over the tip of southern Greenland, providing favourable conditions for lee cyclogenesis or the intensification of pre-existing cyclones (Figs. 7b, c). In fact, 24 % of the westerly CAO events feature cyclogenesis during the day prior to the peak of the event, whereby the respective cyclone centers are required to be located in the Irminger Sea box (cf. green box Fig. 3). This percentage increases to about 30 % when the box is enlarged by 4° to the north.

In association with the upper-level trough, strong westerly winds prevail over southern Greenland at the 500 hPa level between -12 h until the peak of the event (Figs. 7b, c). These winds are crucial in the advection of the CAO airmasses across southern Greenland. The CAO airmasses then descend on the south-western flank of the lee cyclone into the Irminger Sea, whereby they can accelerate considerably.

After the peak of the CAO event, the westerly winds over southern Greenland cease and the center of the lee cyclone translates to the north-east of Iceland (Figs. 7d, e). Thereby, a strong pressure gradient persists to the south of the cyclone center, which gives rise to the rapid eastward advection of the CAO airmasses, in particular towards the coast of Norway.

Prior to easterly CAO events high pressure prevails in the Arctic and over

northern Greenland (Fig. 7f). Furthermore, at lag -24 h two low pressure centres are found in the north-eastern North Atlantic: one to the south of Iceland and a second near the Lofoten archipelago. The anti-cyclonic flow over Greenland and the weak pressure difference between Iceland and the Lofoten archipelago favour northerly winds along most of Greenland's eastern coast. Hence, this configuration is conducive for the long-range transport of Arctic airmasses from Fram Strait to Denmark Strait.

Towards the peak of the CAO event, the low south of Iceland translates to the south-east of Iceland, thereby establishing a strong pressure gradient over Denmark Strait, which is amplified by the barrier effect (Figs. 7g, h). This is in line with high wind speeds found along CAO trajectories from the time of CAO formation onward (cf. section 4.2). Subsequently, the center of the low translates further into the Norwegian Sea (Figs. 7i, k).

The synoptic configuration of the flow over the Nordic Seas in the aftermath of a westerly CAO is favorable for the long-range transport of cold airmasses from Fram Strait southward (cf. Figs. 7d, e). Consequently, 47 (18.5 %) of the westerly CAO events are succeeded by an easterly event within 48 h of the former. In contrast, only 19 (6.8 %) of the easterly events are followed by a westerly event.

4.4.2 Role of anti-cyclones and cyclones in easterly CAO formation

As suggested by the case studies, easterly CAOs can occur in the presence of an anti-cyclone over Greenland (case B), or one or multiple cyclones in the Nordic Seas (case C). Furthermore, the absence of a pronounced upper-level ridge over Greenland in the composites (Figs. 7f–k) indicates that anti-cyclonic flow over Greenland is not present in all cases.

450 In order to stratify the easterly CAO cases according to the anti-cyclonicity
451 of the flow over and around Greenland, I define a Northern Greenland Blocking
452 Index (NGBI). To that end, I extract the timeseries of the area averaged deviation
453 of 500 hPa geopotential height from the zonal mean with the area average taken
454 over the region 80°W–20°W, 68°N–80°N (cf. gray box Fig. 9). The NGBI is
455 obtained from normalizing this timeseries by its standard deviation. This index
456 deviates in two important aspects from indices commonly used to characterise
457 Greenland blocking (e.g., Hanna et al., 2016). First, the area only covers the
458 northern part of Greenland, thereby preventing lee troughs to the south-east of
459 Greenland from polluting the index. The existence of such lee troughs at 500 hPa
460 is evident in the composites of westerly, as well as easterly CAOs (Fig. 7). Second,
461 considering the deviation from the zonal mean ensures that meridional transports
462 are emphasized, whereas zonally uniform states of high or low heights in the
463 latitudinal band of northern Greenland result in neutral values of the index.

464 The NGBI corresponding to a CAO event is defined as the value of the NGBI
465 at the peak of the event, i.e., at lag 0 h. Figure 8 shows the distribution of the NGBI
466 for westerly and easterly CAOs. The distribution of the NGBI for westerly CAOs
467 is clearly shifted towards negative values compared to climatology – a signature of
468 the trough crossing Greenland prior to the CAO event. In contrast, the distribution
469 resembles that of the climatology in the case of easterly CAOs, with the exception
470 that tails are wider. This similarity suggests that a continuous spectrum exists that
471 ranges from cases with an anti-cyclone over Greenland only, such as case B, to
472 cases with a trough over Greenland, potentially with one or multiple cyclones in
473 the Nordic Seas.

474 To quantify how often cyclones are involved in the formation of easterly CAOs,

475 I split the cases into terciles according to the NGBI, yielding about 93 cases in
476 each tercile. For each tercile I compile composites of 500 hPa geopotential height
477 and compute the frequency of cyclones at lags -24 h and 0 h.

478 The lower tercile comprises cases with a main trough to the west of Greenland
479 and a secondary trough east of southern Greenland (Fig. 9a). This secondary
480 trough is related to a high frequency of cyclones to the south-east of Iceland with
481 a maximum frequency of about 80 % at lag 0 h. One day prior to the CAO event
482 local maxima of cyclone frequency are found in the Irminger Sea and off the
483 Lofoten archipelago, akin to the sea level pressure distribution in the composite
484 (Fig. 7f). A similar dipole structure of cyclone frequency at lag -24 h is also
485 evident in the middle tercile (Fig. 9b), however, with no significant trough over
486 Greenland. The upper tercile, in contrast, is characterised by a ridge with its axis
487 located over western Greenland, and therefore anti-cyclonic flow over and around
488 Greenland, as well as low cyclone frequencies (Fig. 9c). Within this classification
489 scheme, case study B clearly belongs to the upper tercile, whereas case study C
490 represents an intermediate case with strongly cyclonic flow over the Nordic Seas
491 and weakly anti-cyclonic flow over northern Greenland, hence, corresponding to
492 the middle tercile.

493 As found in case study B, easterly CAO airmasses can be diverted in opposite
494 directions over the North Atlantic after CAO formation. The CAO airmass fluxes
495 (cf. Fig. 3d) corroborated further that such a splitting is not a peculiarity of this
496 particular case but a climatological feature. A separation of the mass fluxes ac-
497 cording to NGBI terciles reveals that a diversion to the west occurs only in the
498 case of strongly anti-cyclonic flow over Greenland, that is for cases in the upper
499 tercile of the NGBI (not shown). For lower and middle terciles with weak anti-

500 cyclonicity of the flow over Greenland, however, the CAO airmasses are captured
501 by the cyclonic flow over the Nordic Seas and in consequence they are advected
502 to the east towards the British Isles and Norway.

503 The thermodynamic evolution of CAO airmasses prior to CAO formation is
504 by and large independent of the NGBI, i.e., the relative θ -T curves are similar
505 for all terciles (Fig. 5b). After CAO formation, however, the airmasses of the
506 lower tercile experience less diabatic heating and more adiabatic cooling than
507 airmasses of the upper tercile. In fact, the airmasses of the lower tercile undergo
508 an evolution akin to that of westerly CAO airmasses, which is owed to similar
509 synoptic conditions with predominantly cyclonic flow over the Nordic Seas, and
510 hence, similar pathways.

511 **4.5 Surface turbulent heat fluxes**

512 Papritz and Spengler (2016) addressed the question of how much sensible and
513 latent heat CAO airmasses extract from the ocean during the CAO phase. To
514 that end, they interpolated surface sensible and latent heat fluxes to the trajectory
515 positions and accumulated them over the CAO phase of each trajectory. They
516 found Irminger Sea CAO airmasses to extract substantially more latent heat than
517 CAO airmasses in the Nordic Seas with a comparable air-sea potential temperature
518 difference, a circumstance they attributed to the higher sea surface temperature to
519 which Irminger Sea CAO airmasses are exposed. They found further that the total
520 surface turbulent heat flux of Irminger Sea CAO trajectories is dominated by the
521 latent heat flux, whereas in the Nordic Seas the sensible heat flux typically exceeds
522 the latent heat flux.

523 As shown by Papritz et al. (2015), the surface sensible heat flux is propor-
 524 tional to the air-sea potential temperature difference, whereas the latent heat flux
 525 saturates for strong air-sea potential temperature difference at a value essentially
 526 determined by the sea surface temperature. Furthermore, for a CAO airmass,
 527 which is essentially dry at the time of CAO formation, a strongly non-linear rela-
 528 tionship exists between the sea surface temperature and the latent heat flux. This
 529 non-linearity is owed to the approximately exponential relationship between tem-
 530 perature and saturation vapour pressure following the Clausius - Clapeyron rela-
 531 tion. Consequently, the total heat extracted from the ocean by turbulent heat fluxes
 532 depends at first order on the initial intensity of the CAO as measured by the air-sea
 533 potential temperature difference, as well as the sea surface temperature to which
 534 the airmass is exposed (see also Papritz and Spengler (2016) for a more detailed
 535 discussion).

536 I aim here to focus the analysis of Papritz and Spengler (2016) on the Irminger
 537 Sea and refine it by quantifying the extraction of heat from the ocean by west-
 538 erly and easterly CAO airmasses separately (Fig. 10). Westerly and upper tercile
 539 easterly CAO trajectories are the coldest in terms of potential temperature (cf.
 540 Fig. 5a) and, therefore, feature the strongest air-sea potential temperature differ-
 541 ence at $t = 0$ h among all trajectory subsets. Thus, they extract the most sensible
 542 heat in the median (Fig. 10a). Furthermore, westerly and lower tercile easterly
 543 CAO trajectories follow similar pathways after CAO formation into the Nordic
 544 Seas, where waters are colder than further south. Thus, it is unsurprising that they
 545 extract less latent heat than middle and upper tercile easterly CAO trajectories
 546 (Fig. 10b), which are exposed to comparatively warmer waters at lower latitudes.
 547 In fact, the sea surface temperature is the highest for upper tercile easterly CAO

trajectories (not shown) and consequently they extract the most latent heat. However, given the strong diversion of these trajectories, the range of sea surface temperatures to which they are exposed is wider than for the other trajectory subsets. Accordingly, the 10th to 90th –percentile range is the largest for this subset. In the sum, the upper tercile easterly CAO trajectories feature the highest integrated turbulent heat fluxes in the median with the largest 10th to 90th –percentile range among all subsets, whereas westerly and lower tercile easterly CAO trajectories extract the least amount of heat (Fig. 10c).

Surface sensible and latent heat fluxes translate into diabatic warming of the CAO airmass via turbulent upward mixing of the heat in the case of sensible heat fluxes and via condensation, deposition, and freezing in the case of latent heat fluxes. Given that the median surface turbulent heat fluxes are the strongest for the upper tercile easterly CAO trajectories, they undergo the most intense diabatic warming, as supported by the θ – T curves (Fig. 5b). In contrast, westerly and lower tercile easterly CAO trajectories are heated the least and they undergo a very similar thermodynamic evolution owing to roughly equal amounts of heat input.

5 Synthesis and concluding remarks

In this study, I characterised the large-scale synoptic environments favorable for wintertime CAO formation in the Irminger Sea and investigated the pathways of the involved airmasses, as well as their characteristic properties. To this end, I made use of kinematic trajectories, derived from the three dimensional winds in ERA-Interim, to sample Irminger Sea CAO airmasses.

571 I identified three distinct synoptic environments conducive for CAO formation
572 in the Irminger Sea. These environments and the associated transport pathways of
573 the airmasses before and after CAO formation are schematically summarised in
574 Fig. 11. Our principal findings in regard of these environments and the properties
575 of the associated CAO airmasses are:

576 1. In the westerly environment (Fig. 11a), an upper-level trough, with its axis
577 crossing Greenland's plateau, establishes flow towards southern Greenland
578 and strong westerly winds at its crest. Hence, CAO airmasses from the
579 Canadian Arctic, whereof more than 50 % originate in the free troposphere
580 and do not ascend substantially prior to crossing Greenland, are forced to
581 overflow southern Greenland and descend in its lee. The most intense cli-
582 matological downslope mass fluxes are focused on the Ammassalik region
583 and Greenland's southern tip. Moreover, the eastward motion of the upper-
584 level trough is conducive for lee cyclogenesis or the intensification of a pre-
585 existing cyclone in the lee of Greenland. In fact, cyclone tracks revealed
586 that almost one third of the westerly CAO events feature lee cyclogenesis.
587 As the lee cyclone propagates into the Nordic Seas, the CAO airmasses are
588 rapidly exported north-eastwards on the cyclone's southern flank.

589 2. A major fraction of easterly CAO airmasses originates in the interior Arctic
590 and is transported all the way from Fram Strait along Greenland's eastern
591 coast towards Denmark Strait. In the cyclonic environment (Figs. 11b), this
592 long-range transport is established by one or two sequential extratropical cy-
593 clones located ahead of an upper-level trough, whereas in the anti-cyclonic
594 environment (Figs. 11c) the transport is due to anti-cyclonic flow over and

595 around Greenland. Contributions from katabatic drainage flows from north-
596 ern Greenland merge with the southbound flow of barrier-wind enhanced
597 CAO airmasses, whereby in the case of the cyclonic environment, addition-
598 ally also marine airmasses from the Barents and Nordic seas contribute.

599 After CAO formation, the airmasses follow a similar pathway as in the west-
600 erly environment in the cyclonic case, albeit reaching less far north along
601 the Norwegian coast. In contrast, a bifurcation occurs in the anti-cyclonic
602 case with some of the airmasses not being advected eastwards but towards
603 Newfoundland and Labrador instead.

604 3. The westerly environment bears similarities to the synoptic configuration
605 identified by Kolstad et al. (2009), whereas the easterly environments are
606 clearly distinct. The cyclonic and anti-cyclonic easterly environments rep-
607 resent limiting cases of an intermediate spectrum with synoptic features
608 common to both environments.

609 4. The synoptic configuration of the flow over the Nordic Seas in the aftermath
610 of a westerly CAO event is conducive for the transport of airmasses along
611 Greenland's eastern coast. Consequently, almost 20 % of the westerly CAO
612 events are succeeded by a cyclonic easterly event within 48 h after the peak
613 of the westerly event.

614 5. About 10 % of the CAO trajectories experience high wind speeds in excess
615 of 20 m s^{-1} during the CAO phase, which are associated with westerly tip
616 jets in the case of westerly CAOs, and barrier winds in the case of easterly
617 cyclonic CAOs. The intense winds imply a high potential of these airmasses
618 to extract sensible and latent heat from the ocean.

619 6. The amount of heat extracted from the ocean, and hence the diabatic tem-
620 perature increase after CAO formation, depends not only on the air-sea po-
621 tential temperature difference at the time of CAO formation, but also on the
622 subsequent pathway of the airmasses, which is set by the respective synoptic
623 environment. Specifically, airmasses associated with easterly anti-cyclonic
624 CAO events extract - when accumulated over the entire CAO phase - the
625 most heat from the ocean, which is due to their exposition to warmer wa-
626 ters along their pathway; this results in the strongest diabatic temperature
627 increase among Irminger Sea CAO airmasses.

628 The formation of CAOs is closely related to the occurrence of barrier winds.
629 Harden et al. (2011) identified two distinct regimes of barrier winds near Den-
630 mark Strait, a cold and a warm regime. Cold barrier winds occur in the presence
631 of a cyclone in the Norwegian Sea prior to the event, which promotes the south-
632 ward transport of cold airmasses along Greenland's east coast, and the subsequent
633 passage of a cyclone with its core near Iceland, hence, resembling the easterly
634 cyclonic CAO regime. This indicates that cold barrier winds are closely related
635 to easterly cyclonic CAOs, whereby the barrier flow channels CAO airmasses
636 through Denmark Strait. Interestingly, also the synoptic environments of warm
637 barrier winds and westerly CAOs bear a certain similarity with a cyclone located
638 in the central Irminger Sea. In cases of a concomitant westerly CAO and warm
639 barrier winds, strong north-south contrasts of temperature and air-sea heat flux
640 forcings would ensue over the Irminger Sea, implying high baroclinicity.

641 The Irminger Sea is an important genesis region for cyclones undergoing
642 strong intensification and propagating north-eastwards into the Nordic Seas (Dacre
643 and Gray, 2009). Here, I have shown that westerly and easterly cyclonic CAO air-

644 masses contribute to the cold sector of such cyclones. As surface sensible heating
645 and latent heat release in CAOs enhance lower tropospheric baroclinicity (e.g.,
646 Papritz and Spengler, 2015), I hypothesize that a positive feedback exists between
647 CAO formation and the intensification of cyclones striking the Nordic Seas. Thus,
648 future work should address these feedbacks in numerical process studies, and then
649 assess the relevance of CAO airmasses in enhancing cyclone intensification clima-
650 tologically.

651 ACKNOWLEDGEMENTS

652 I would like to thank K. Våge (University of Bergen) for helpful discussions
653 and three anonymous reviewers for their insightful comments. Furthermore, I am
654 grateful to the Institute for Atmospheric and Climate Science of ETH Zürich for
655 kindly providing access to their computational resources, and the European Cen-
656 tre for Medium-Range Weather Forecasts for making the ERA-Interim reanaly-
657 sis available. I acknowledge support by the Swiss National Science Foundation
658 (SNSF), grant P2EZP2_162267.

References

- Buckley, M. W., and J. Marshall, 2016: Observations, inferences, and mechanisms of atlantic meridional overturning circulation variability: A review. *Rev. Geophys.*, **54**, 5–63, doi:10.1002/2015RG000493.
- Dacre, H. F., and S. L. Gray, 2009: The spatial distribution and evolution characteristics of North Atlantic cyclones. *Mon. Wea. Rev.*, **137**, 99–115, doi:10.1175/2008MWR2491.1.
- Dee, D., and Coauthors, 2011: The ERA-Interim reanalysis: configuration and performance of the data assimilation system. *Quart. J. Roy. Meteor. Soc.*, **137**, 553–597, doi:10.1002/qj.828.
- Doyle, J. D., and M. A. Shapiro, 1999: Flow response to large-scale topography: The Greenland tip jet. *Tellus*, **51A**, 728–748, doi:10.1034/j.1600-0870.1996.00014.x.
- Hanna, E., T. E. Cropper, R. J. Hall, and J. Cappelen, 2016: Greenland Blocking Index 1851-2015: a regional climate change signal. *Int. J. Climatol.*, **36**, 4847–4861, doi:10.1002/joc.4673.
- Harden, B. E., and I. A. Renfrew, 2012: On the spatial distribution of high winds off southeast Greenland. *Geophys. Res. Lett.*, **39**, L14 806, doi:10.1029/2012GL052245.
- Harden, B. E., I. A. Renfrew, and G. N. Petersen, 2011: A climatology of wintertime barrier winds off southeast Greenland. *J. Climate*, **24**, 4701–4717, doi:10.1175/2011JCLI4113.1.

- 681 Heinemann, G., and T. Klein, 2002: Modelling and observations of the kata-
682 batic flow dynamics over Greenland. *Tellus A*, **54**, 542–554, doi:10.1034/j.
683 1600-0870.2002.201401.x.
- 684 Hurrell, J. W., 1995: Decadal trends in the North Atlantic Oscillation: Regional
685 temperatures and precipitation. *Science*, **269**, 676–679, doi:10.1126/science.
686 269.5224.676.
- 687 Jahnke-Bornemann, A., and B. Brümmer, 2009: The Iceland-Lofotes pressure
688 difference: different states of the North Atlantic low-pressure zone. *Tellus A*,
689 **61**, 466–475, doi:10.1111/j.1600-0870.2009.00401.x.
- 690 Kolstad, E. W., T. J. Bracegirdle, and I. A. Seierstad, 2009: Marine cold-air
691 outbreaks in the North Atlantic: temporal distribution and associations with
692 large-scale atmospheric circulation. *Clim. Dyn.*, **33**, 187–197, doi:10.1007/
693 s00382-008-0431-5.
- 694 Moore, G. W. K., R. S. Pickart, and I. A. Renfrew, 2008: Buoy observations from
695 the windiest location in the world ocean, Cape Farewell, Greenland. *Geophys.*
696 *Res. Lett.*, **35**, L18 802, doi:10.1029/2008GL034845.
- 697 Moore, G. W. K., and I. A. Renfrew, 2005: Tip jets and barrier winds: A
698 QuikSCAT climatology of high wind speed events around Greenland. *J. Cli-*
699 *mate*, **18**, 3713–3725, doi:10.1175/JCLI3455.1.
- 700 Nansen, F., 1912: Das Bodenwasser und die Abkühlung des Meeres. *Internationale*
701 *Revue der Gesamten Hydrobiologie und Hydrographie*, **5**, 1–42.
- 702 Oltmanns, M., F. Straneo, G. W. K. Moore, and S. H. Mernild, 2014: Strong

- 703 downslope wind events in Ammassalik, southeast Greenland. *J. Climate*, **27**,
704 977–993, doi:10.1175/JCLI-D-13-00067.1.
- 705 Papritz, L., S. Pfahl, H. Sodemann, and H. Wernli, 2015: A climatology of cold
706 air outbreaks and their impact on air-sea heat fluxes in the high-latitude South
707 Pacific. *J. Climate*, **28**, 342–364, doi:10.1175/JCLI-D-14-00482.1.
- 708 Papritz, L., and T. Spengler, 2015: Climatological analysis of the slope of isen-
709 tropic surfaces and its tendencies over the North Atlantic. *Quart. J. Roy. Meteor.*
710 *Soc.*, **141**, 3226–3238, doi:10.1002/qj.2605.
- 711 Papritz, L., and T. Spengler, 2016: A Lagrangian climatology of wintertime cold
712 air outbreaks in the Irminger and Nordic seas and their role in shaping air-sea
713 heat fluxes. *J. Climate*, in review.
- 714 Petersen, G. N., H. Olafsson, and J. E. Kristjansson, 2003: Flow in the lee
715 of idealized mountains and Greenland. *J. Atmos. Sci.*, **60**, 2183–2195, doi:
716 10.1175/1520-0469(2003)060<2183:FITLOI>2.0.CO;2.
- 717 Petersen, G. N., I. A. Renfrew, and G. W. K. Moore, 2009: An overview of bar-
718 rier winds off southeastern Greenland during the Greenland Flow Distortion
719 experiment. *Quart. J. Roy. Meteor. Soc.*, **135**, 1950–1967, doi:10.1002/qj.455.
- 720 Pickart, R. S., M. A. Spall, M. H. Ribergaard, G. W. K. Moore, and R. F. Milliff,
721 2003a: Deep convection in the Irminger Sea forced by the Greenland tip jet.
722 *Nature*, **424**, 152–156, doi:10.1038/nature01729.
- 723 Pickart, R. S., F. Straneo, and G. W. K. Moore, 2003b: Is Labrador Sea wa-

724 ter formed in the Irminger basin? *Deep Sea Res. I*, **50**, 23–52, doi:10.1016/
725 S0967-0637(02)00134-6.

726 Sampe, T., and S.-P. Xie, 2007: Mapping high sea winds from space: a
727 global climatology. *Bull. Amer. Meteor. Soc.*, **88**, 1965–1978, doi:10.1175/
728 BAMS-88-12-1965.

729 Sprenger, M., and H. Wernli, 2015: The Lagrangian analysis tool LA-
730 GRANTO - version 2.0. *Geosci. Model Dev.*, **8**, 1893–1943, doi:10.5194/
731 gmdd-8-1893-2015.

732 Våge, K., T. Spengler, H. C. Davies, and R. S. Pickart, 2009a: Multi-event analy-
733 sis of the westerly Greenland tip jet based upon 45 winters in ERA-40. *Quart.*
734 *J. Roy. Meteor. Soc.*, **135**, 1999–2011, doi:10.1002/qj.488.

735 Våge, K., and Coauthors, 2009b: Surprising return of deep convection to the
736 subpolar North Atlantic Ocean in winter 2007-2008. *Nat. Geosci.*, **2**, 67–72,
737 doi:10.1038/NGEO382.

738 Våge, K., and Coauthors, 2011: The Irminger Gyre: circulation, convection, and
739 interannual variability. *Deep Sea Res. I*, **58**, 590–614, doi:10.1016/j.dsr.2011.
740 03.001.

741 Wanner, H., S. Brönnimann, C. Casty, D. Gyalistras, J. Luterbacher, C. Schmutz,
742 D. B. Stephenson, and E. Xoplaki, 2001: North Atlantic Oscillation - Concepts
743 And Studies. *Surv. Geophys.*, **22**, 321–381, doi:10.1023/A:1014217317898.

744 Wernli, H., and C. Schwierz, 2006: Surface cyclones in the ERA-40 dataset (1958-

745 2001). Part I: Novel identification method and global climatology. *J. Atmos.*
746 *Sci.*, **63**, 2486–2507, doi:10.1175/JAS3766.1.

747 Woollings, T., L. Papritz, C. Mbengue, and T. Spengler, 2016: Diabatic heating
748 and jet stream shifts: A case study of the 2010 negative North Atlantic Oscilla-
749 tion winter. *Geophys. Res. Lett.*, **43**, 9994–10 002, doi:10.1002/2016GL070146.

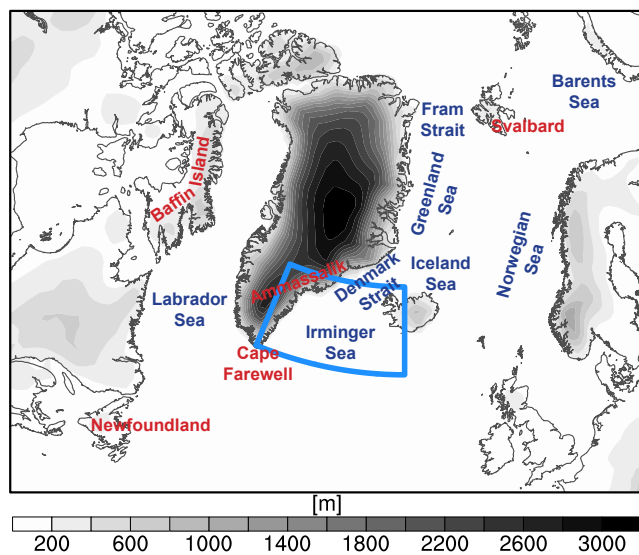


Figure 1: Location names and topography of the study region as represented in ERA-Interim. The blue box shows the starting region for the trajectories.

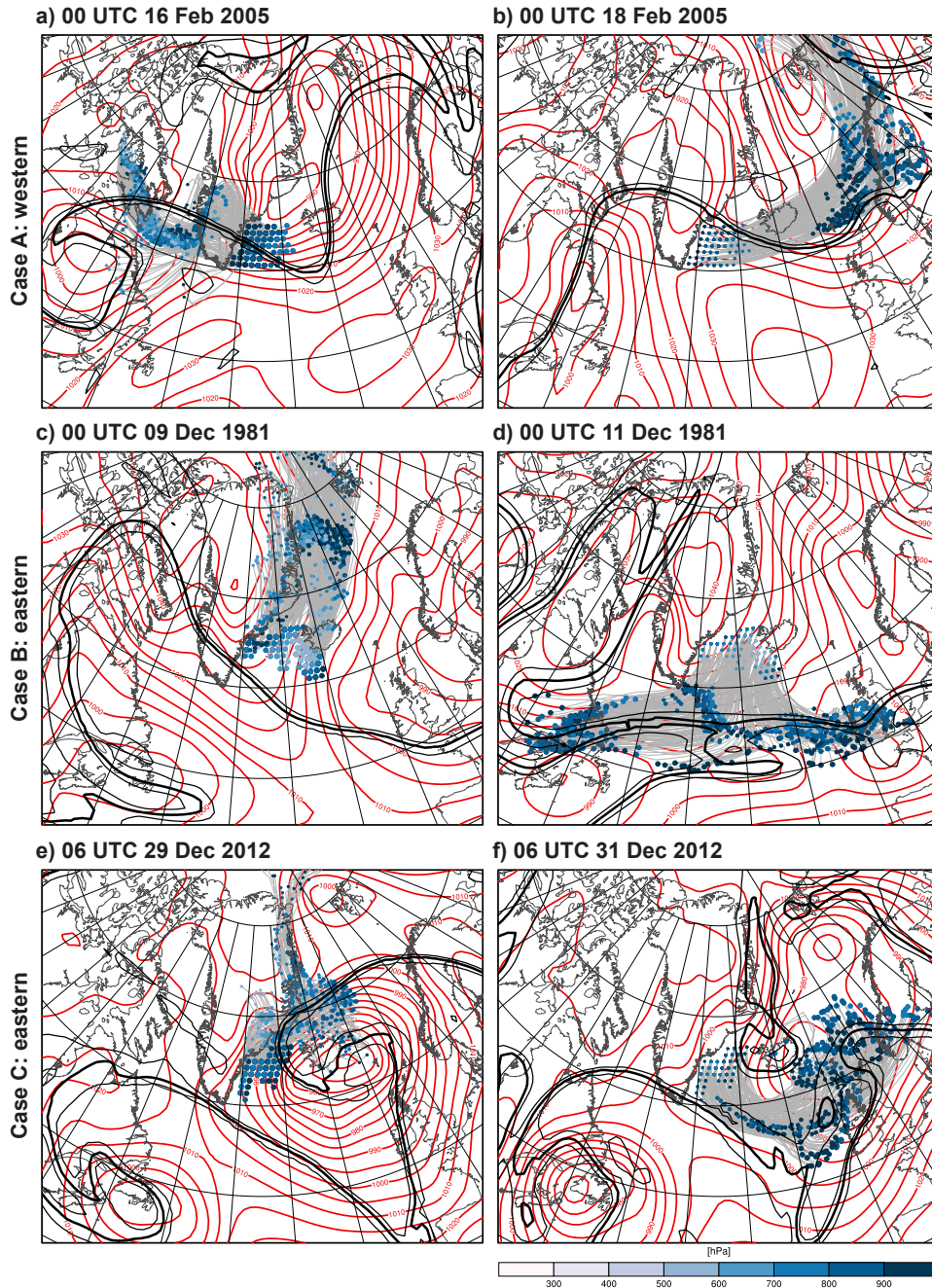


Figure 2: Synoptic configurations for selected westerly (A) and easterly (B, C) CAO events. Shown are sea level pressure in intervals of 5 hPa (red) and PV on the 310 K isentropic surface from 1 pvu to 3 pvu in intervals of 1 pvu (black, 2 pvu line bold) (a, c, e) at the peak of the events and (b, d, f) 2 days after (cf. dates at the top of each panel). CAO trajectories in the time interval (a, c, e) $-48 \text{ h} \leq t \leq 0 \text{ h}$ and (b, d, f) $0 \text{ h} \leq t \leq 48 \text{ h}$ are shown in gray with dots at the beginning (small dots), middle (medium dots), and end (large dots) of the respective time intervals. Colors indicate the pressure of the trajectories at the respective times. Note that only trajectories are shown with their basetime corresponding to the peak of the event.

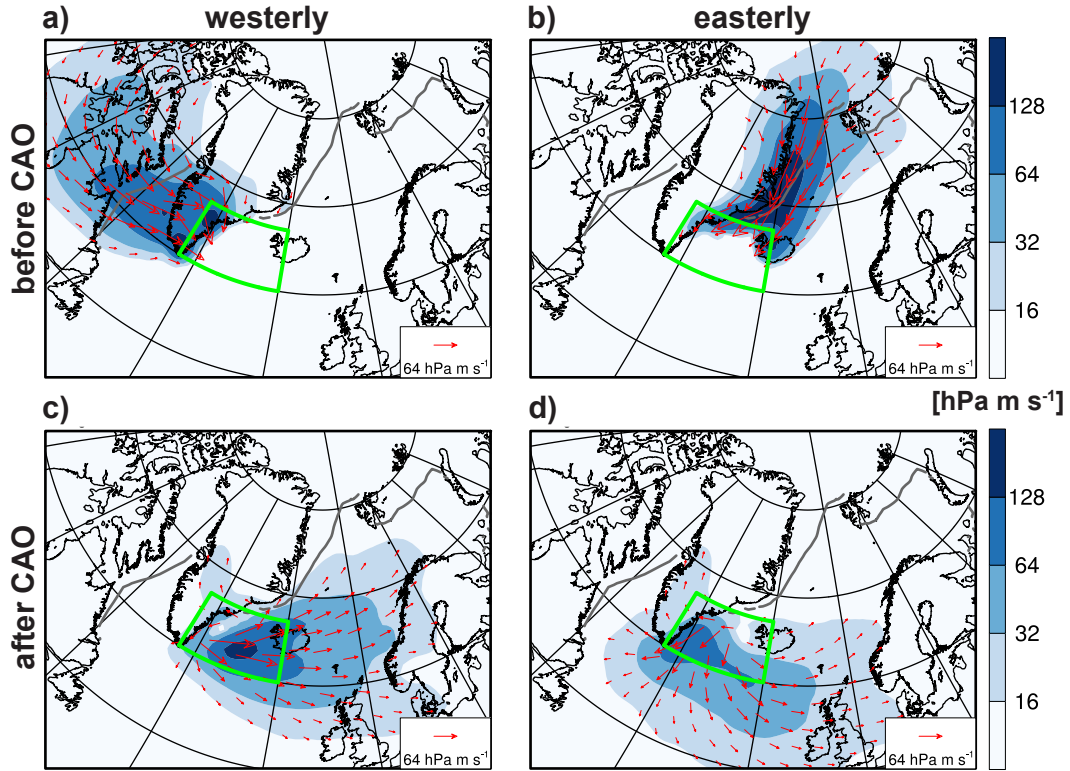


Figure 3: Mean horizontal mass fluxes (vectors) and their magnitude (shading) associated with westerly (a, c) and easterly (b, d) CAO trajectories (a, b) prior to ($-96 \text{ h} \leq t < 0 \text{ h}$) and (c, d) after ($0 \text{ h} \leq t \leq 96 \text{ h}$) CAO formation. The green box outlines the CAO formation area from which backward and forward trajectories are started. The gray contour indicates the sea ice edge (50 % sea ice concentration).

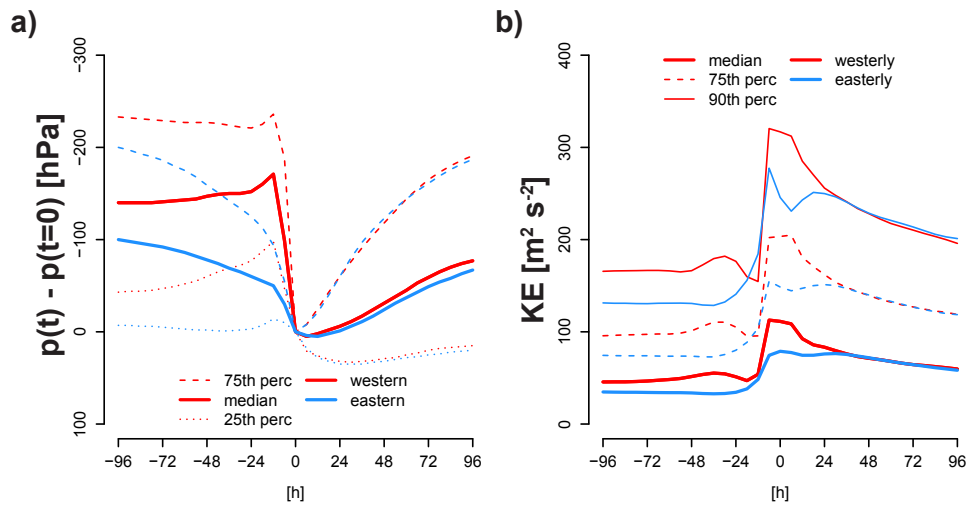


Figure 4: Evolution of (a) pressure relative to the time of CAO formation ($t = 0$ h), and (b) specific kinetic energy for CAO trajectories following the westerly (red) and easterly (blue) pathways. Shown are for (a) the 25th-percentile (dotted), the median (solid), and the 75th-percentile (dashed), and for (b) the median (solid), the 75th-percentile (dashed), and the 90th-percentile (thin solid).

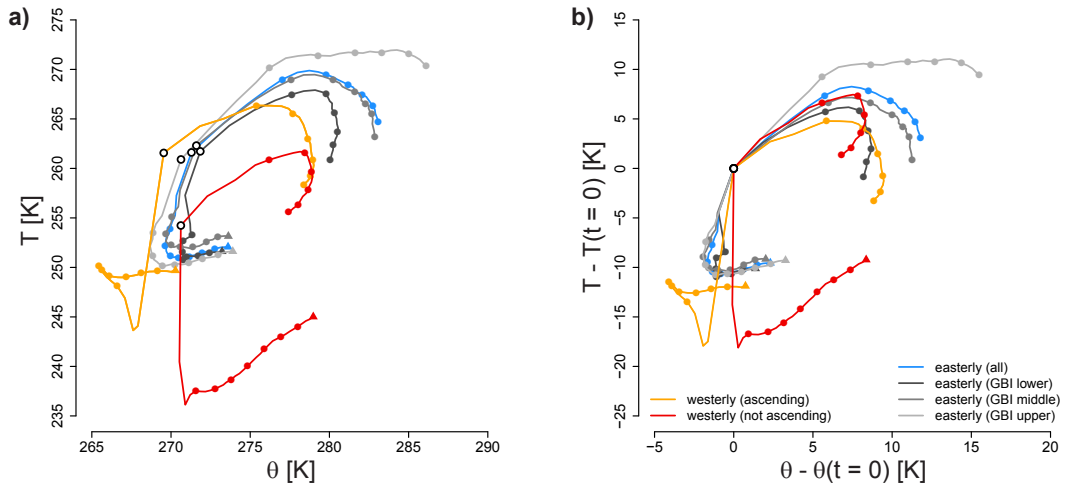


Figure 5: θ – T diagram for westerly ascending (orange) and non-ascending (dark red), as well as easterly (blue) median CAO trajectories. The sets of ascending (non-ascending) trajectories comprise the trajectories whose pressure at $t = -48$ h is above (below) the median of westerly CAO trajectories. In addition, easterly CAO trajectories are split into lower (dark gray), middle (gray) and upper (light gray) terciles of the Greenland Blocking Index (cf. section 4.4.2). Values are (a) absolute and (b) relative to $t = 0$ h and they are shown for $-192 \text{ h} \leq t \leq 144 \text{ h}$ in 6-hourly intervals with dots every 24 h. Times $t = -192 \text{ h}$ and $t = 0 \text{ h}$ are highlighted by triangles and black circles, respectively.

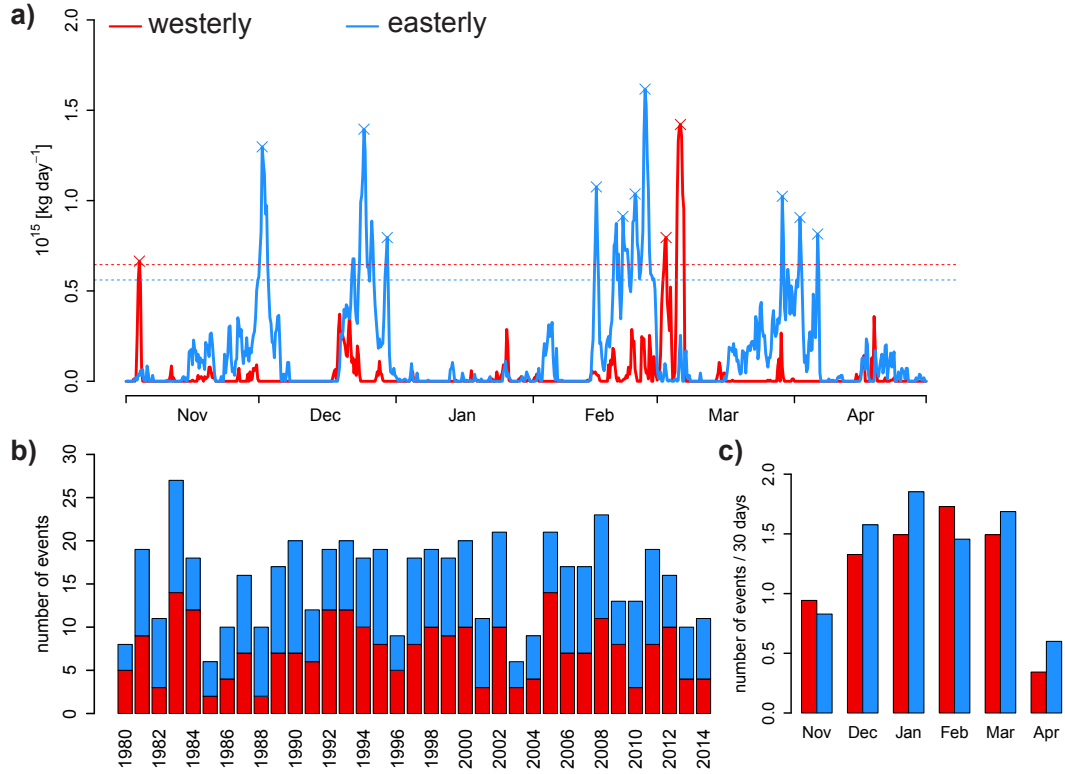


Figure 6: (a) Timeseries of formation rates of westerly (red) and easterly (blue) CAOs in units of $10^{15} \text{ kg day}^{-1}$ for extended winter 2009 / 2010. Crosses show CAO events and dashed lines indicate the 95th-percentiles of the formation rates. (b) Inter-annual and (c) month-to-month variability of CAO events. The month-to-month variability is normalized in order to account for the different lengths of the months.

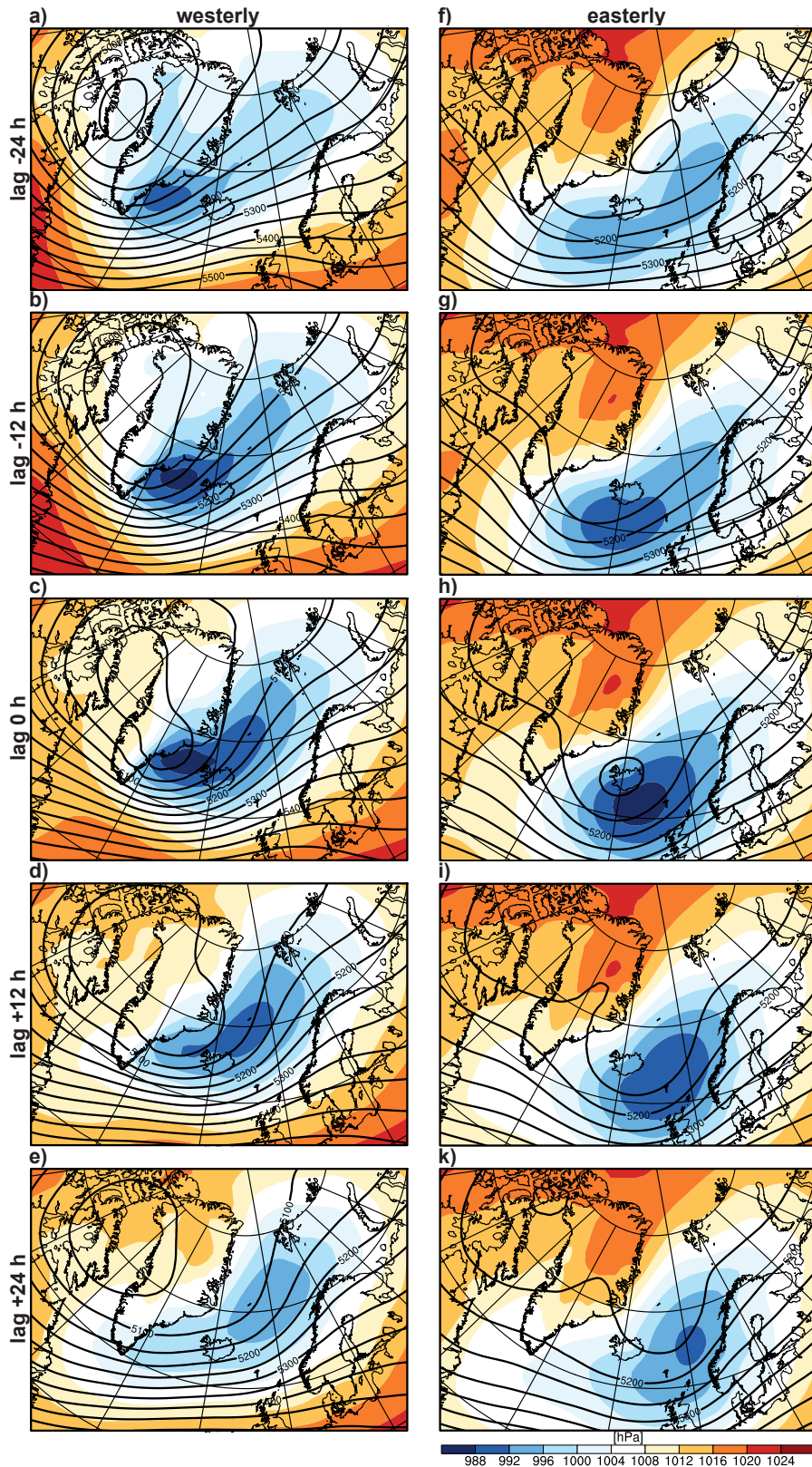


Figure 7: Lag composites for westerly (a–e) and easterly (f–k) CAO events showing sea-level pressure (shading) and 500 hPa geopotential height (black). Composites are shown at lags (a, f) -24 h, (b, g) -12 h, (c, h) 0 h, (d, i) 12 h and (e, k) 24 h relative to the peaks of the CAO events.

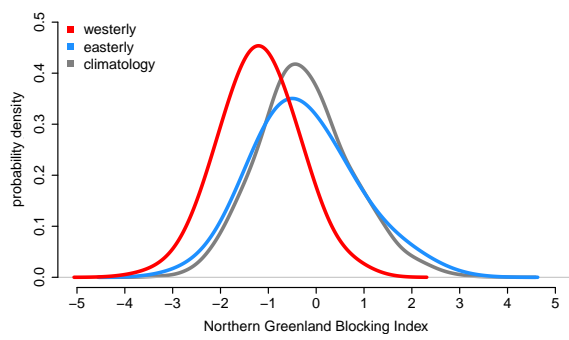


Figure 8: Probability density of the NGBI for extended winters (gray), westerly (red) and easterly (blue) CAO events.

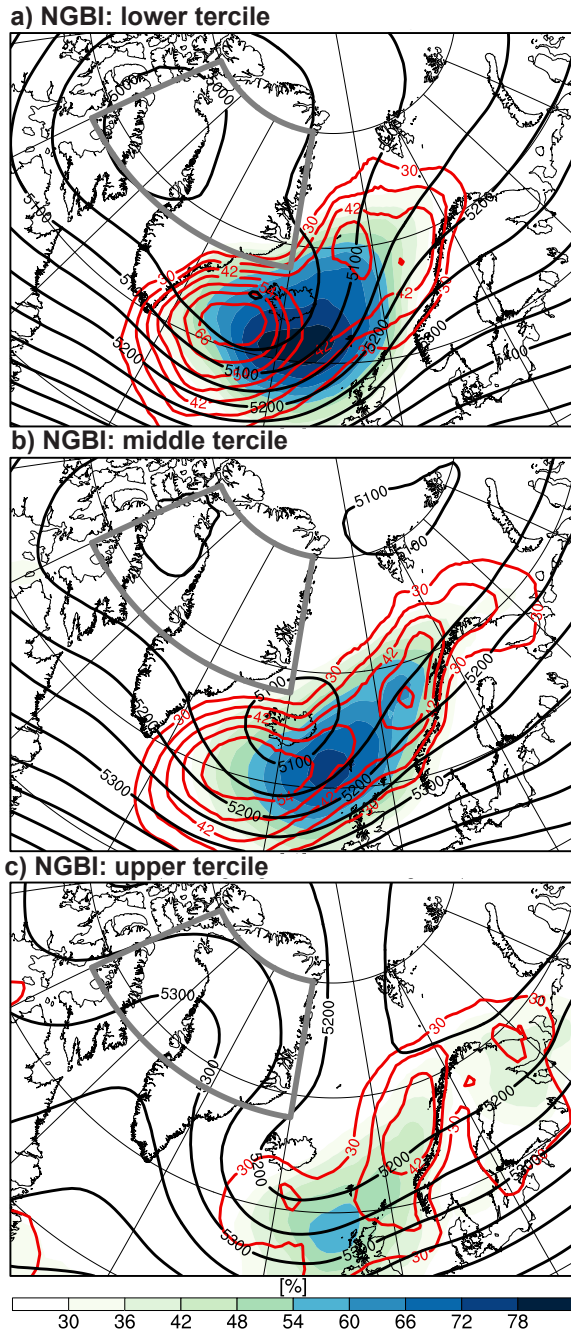


Figure 9: Cyclone frequency for easterly CAOs in % at lag -24 h (red, from 30 % in intervals of 6 %) and 0 h (shading) stratified into (a) lower, (b) middle, and (c) upper terciles of the NGBI. Composite 500 hPa geopotential height at lag 0 h is shown by black contours. The region used for the NGBI calculation is outlined by the gray box.

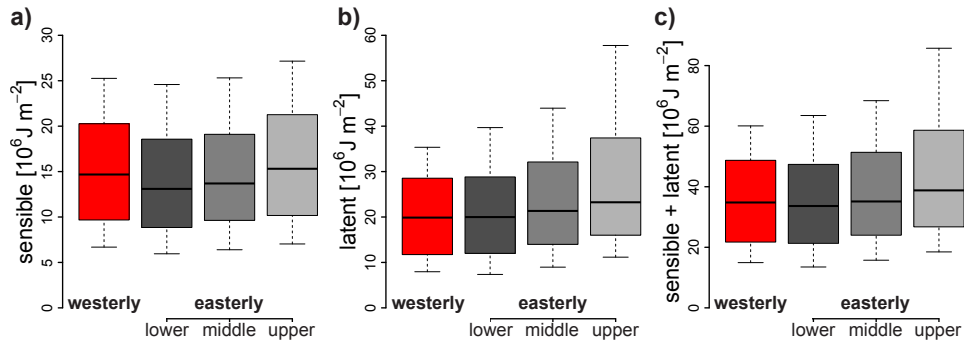


Figure 10: Boxplots of (a) sensible, (b) latent, and (c) sensible and latent heat fluxes accumulated over the CAO phase of westerly (red) and lower (dark gray), middle (gray), and upper (light gray) terciles of easterly CAO trajectories corresponding to CAO events. Whiskers indicate 10th and 90th –percentiles, respectively.

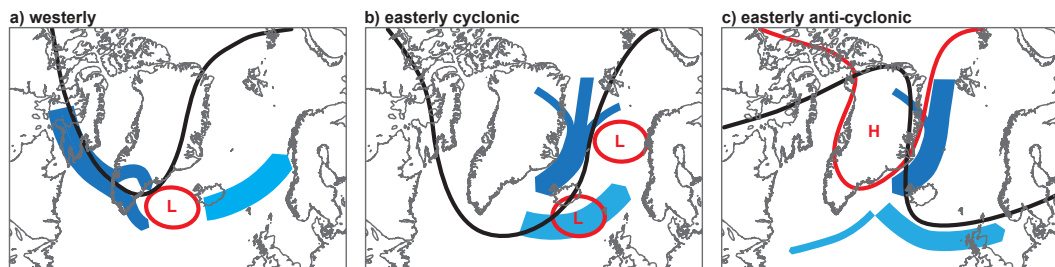


Figure 11: Schematic summarizing synoptic environments favorable for CAO formation in the Irminger Sea. The environments are (a) westerly, (b) easterly cyclonic, and (c) easterly anti-cyclonic. Shown are a typical contour line of 500 hPa geopotential height (black), surface cyclones and anti-cyclones (red) all at the peak of CAO events. In addition, pathways of CAO airmasses prior to (dark blue) and after (light blue) CAO formation are depicted.